A Probabilistic Diffusion Weld Modeling Framework

A probabilistic modeling framework realistically accounts for manufacturing variability and successfully models bond impact strength in Ti-6Al-4V

BY V. R. DAVÉ, I. J. BEYERLEIN, D. A. HARTMAN, AND J. M. BARBIERI

ABSTRACT. Physics-based modeling of critical diffusion welds is problematic at best and, in practice, semi-empirical approaches are employed. This work reviews existing pore closure models identifying their shortcomings vis-à-vis actual manufacturing environments. A framework is developed that incorporates realistic manufacturing process attributes such as surface topography into pore closure models. Relevant quantities are represented as distribution functions instead of deterministic values, and manufacturing attributes are then correlated to parameters in these distribution functions. Using a Monte Carlo approach, the distribution of residual joint porosity as a function of both manufacturing attributes and bond process conditions (time, pressure, and temperature) can be derived. Existing models do not capture joint strength, so an additional objective of this work is to model the relationship between residual joint porosity and joint impact strength by applying probabilistic failure models. Finally, this overall approach is applied to model impact strength data of diffusion welds in Ti-6Al-4V.

Introduction

Diffusion welding has been successfully applied to critical components for the past 30-plus years. For demanding applications such as gas turbine engines, there are extreme quality requirements and significant process control challenges (Refs. 1–4). As a practical matter, manufacturers have resorted to empirical process development, occasionally augmented by process modeling. Physically motivated analytical approaches have seldom met with success in accelerating development efforts. The reasons for this are numerous but include:

1) No clear methodology for incorporating realistic manufacturing process attributes into physically motivated models

2) The lack of a linkage between pore closure models and mechanical properties

3) Insufficient or inaccurate materials data to evaluate all the material constants in pore closure models

Although infrequently used in the past, analytical models are useful. Diffusion weld quality assurance for critical applications is presently based on exhaustive and expensive nondestructive and destructive examination. Due to the extreme consequences of an in-service failure, this conservative strategy is adopted. From a manufacturing perspective, in-process quality assurance is desired, capturing all relevant manufacturing process attributes. From a design engineering perspective, assessment of component reliability as a function of manufacturing attributes is needed while minimizing specimen testing. For example, the fracture and fatigue properties of diffusion welded articles exhibit a strong dependence on residual porosity level, pointing to the need for probabilistic approaches to characterize the dependence of mechanical properties on porosity. Achieving these objectives would significantly reduce manufacturing cost and reduce the engineering effort needed to qualify new designs or processes. Improved modeling can therefore benefit manufacturing quality assurance as well as design reliability, and this work represents an initial effort along these lines. This is done by first relating machining process parameters to an initial porosity distribution, then allowing pore closure models to operate on the initial pore distribution to give a final pore distribution, and, finally, making the link between porosity and weld impact strength. Weld impact strength is chosen because it conservatively assesses weld quality.

V. R. DAVÉ and D. A. HARTMAN are with the Nuclear Materials and Technology Div., and I. J. BEYERLEIN is with the Theoretical Div., Los Alamos National Laboratory, Los Alamos, N. Mex. J. M. BARBIERI is with United Technologies Corp., E. Hartford, Conn.

KEY WORDS

Diffusion Welding
Titanium
Porosity
Probabilistic Model
Monte Carlo
Topography

Review of Existing Pore Closure Models for Diffusion Welding and Their Shortcomings

The first conceptual process model by King and Owczarski (Ref. 5) had four stages — Fig. 1: 1) initial contact, 2) attainment of intimate interfacial contact, 3) grain boundary diffusion/migration, and, finally, 4) volume diffusion. Initial contact is limited to a few asperities, followed by Stage 1, in which the asperities are crushed. Stage 2 involves grain boundary diffusion and migration, whereas Stage 3 consists of volume diffusion to isolated voids. King and Owczarski offered a conceptual framework but did not quantitatively model pore closure. Kellerer and Milacek (Ref. 6) also identified creep and bulk diffusion as mechanisms through which intimate surface contact is developed. Another early work by Hamilton (Ref. 7) proposed that the diffusion welding process consists of four steps: 1) development of intimate interfacial contact, 2) formation of the metallic bond, 3) interdiffusion, and 4) recrystallization/grain growth. Hamilton modeled pore closure dominated by plastic flow with asperity crushing and successfully identified the pressure required to achieve joint tensile strengths approaching base material properties. Ironically, this early work offered predictive capability with respect to joint strength, whereas in subsequent works, this link to mechanical properties is absent.

The first quantitative pore closure

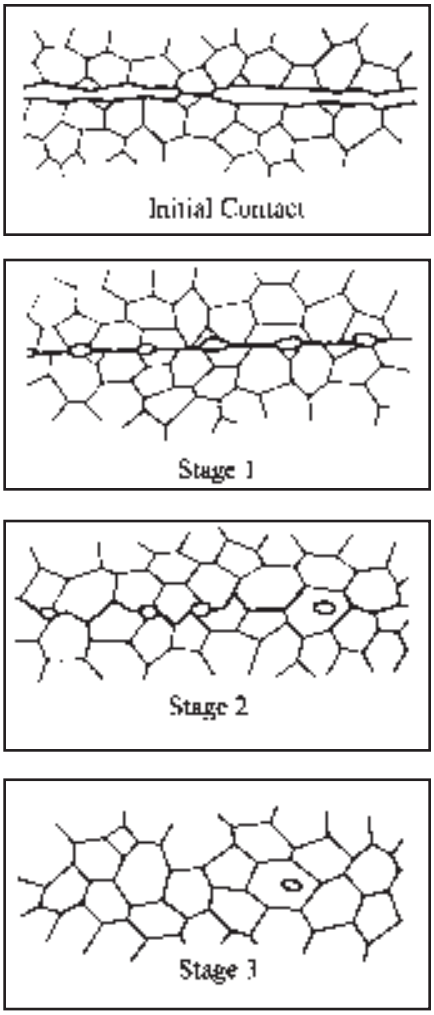

Fig. 1 — Schematic illustrating stages of diffusion welding.

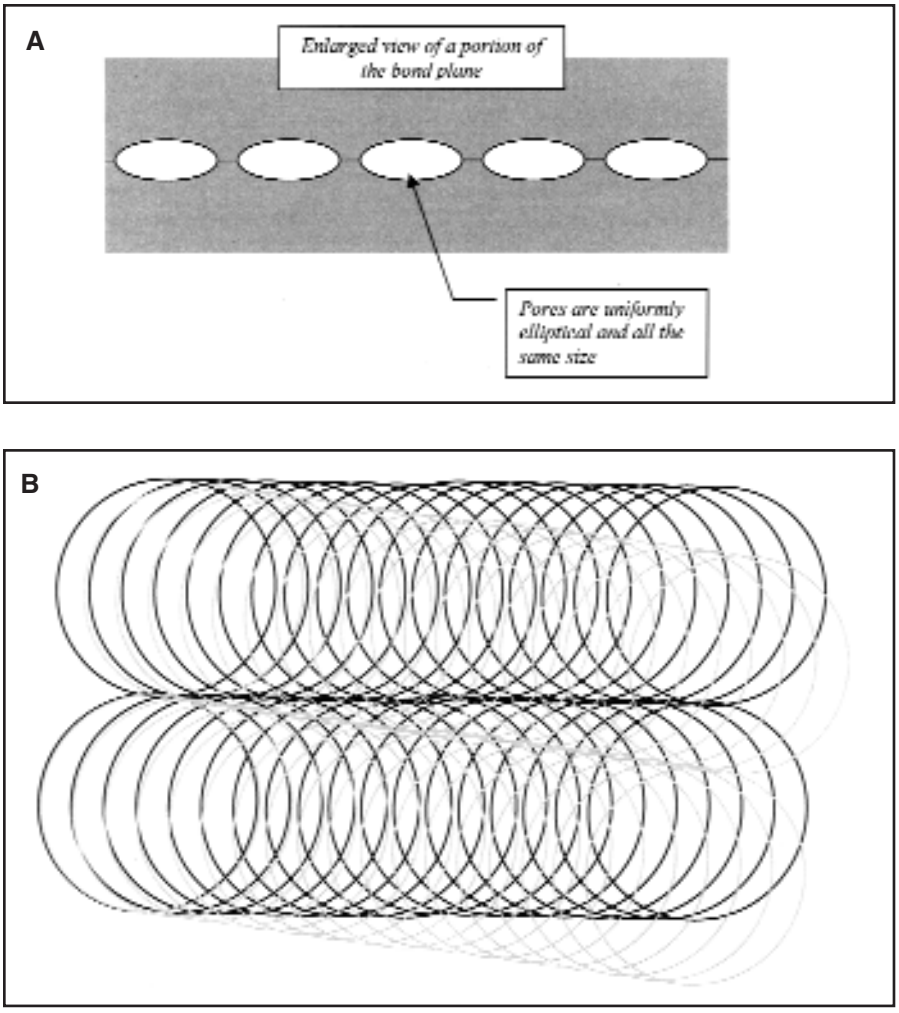

Fig. 2 — Weld surface topography. A — Idealized but inaccurate representation of pore distribution; B — schematic representation of the intersection of cutter marks of two machined surfaces.

model including multiple mechanisms was by Garmong, Paton, and Argon in 1975 (Ref. 8). Garmong et al. included the effects of surface topography by characterizing long and short wavelength surface features and proposed multiple local pore closure mechanisms, namely creep and vacancy diffusion. They were also the first to realize surface waviness (long wavelength features) could dominate the time required to attain interfacial contact but that local pore closure determines the rate of final densification and the residual porosity distribution. The physics of pore sintering based on surface energy and power law creep mechanisms is traceable to Coble (Ref. 9) and Wilkinson and Ashby (Ref. 10). Coble (Ref. 9) examined both surface energy and creep as driving forces, whereas Wilkinson and Ashby (Ref. 10) examined in greater detail the influence of creep.

The next significant extensions to pore closure models are found in a series of works first by Derby and Wallach (Refs. 11–14) and later by Hill and Wallach (Ref. 15). These models incorporate multiple pore closure mechanisms dominant at various stages in the welding process. Table 1 outlines these mechanisms and their underlying physical driving forces (Ref. 15). Although this series of models culminating in Ref. 15 significantly advanced understanding of pore closure mechanisms, the claim of the authors in Ref. 15, namely that modeling can "…virtually eliminate the need to experimentally optimize bonding conditions," is unfortunately not realized in industrial practice.

Additional models include Pilling et al. (Ref. 16) and Guo and Ridley (Ref. 17), who examined the diffusion welding of Ti-6Al-4V. Pilling et al. (Ref. 16) considered creep as influenced by effect of grain size. Guo and Ridley expanded upon this work to incorporate diffusion effects and the role of void shape and phase proportions (e.g., α and β phases). Takahaski and Inoue (Ref. 18) examined the method in which creep and diffusion terms are combined under various loading conditions. They found that void shrinkage depends on macroscopic mechanical constraint, i.e., boundary conditions imposed by tooling.

There is significant former Soviet Union work on diffusion welding mechanisms relevant to modeling. References 19 and 20 identified the importance of the local strain at the interface. One work examined relaxation of machining-induced residual stresses and found these strain rates to be twice as large as bulk creep rates (Ref. 21). Additionally the effects of rolling texture on joining kinetics have been examined for Alloy VT6 (aerospace grade Ti-6Al-4V) in Ref. 22. Several works examined the effect of residual gas at the weld interface, the dissolution kinetics of surface oxides, and the dependence of weld strength on the amount of surface oxide initially present (Refs. 23–25, respectively).

Now the shortcomings of current pore closure models are critically examined. Although this work does not address all of

Table 1 — Pore Closure Mechanisms and Their Underlying Physical Driving Forces

	Pore Closure Mechanism	Physical Driving Force(s)
1	Plastic yielding of asperities during initial contact	Mostly determined by stress state at bond
2	Creep	
3	Surface diffusion from a surface source to a neck (intersection region separating two pores)	Differences in surface curvature, so these mechanisms cease when pores no longer have varying radii of curvature
4	Volume diffusion from a surface source to a neck	
5	Vapor-phase transport from a surface source to a neck	
6	Diffusion along the bond interface or a grain boundary from interfacial sources to a neck	Chemical potential gradient, which will be influenced by local stress state
7	Volume diffusion from interfacial sources to a neck	

these, the modeling framework presented here is a useful starting point in making pore closure models more realistic. The most limiting shortcoming is that current models do not address the issue of joint strength. In solid-state diffusion welds the weld impact strength is the most sensitive measure of weld imperfections such as residual porosity or contamination (Ref. 26). The impact strength can drop significantly due to small fractions of residual porosity. Other than the early work by Hamilton (Ref. 7), the authors are not aware of a single work that attempts to model any aspect of diffusion weld mechanical properties. The probabilistic failure model in this present work is, therefore, the first of its kind as applied to diffusion welding.

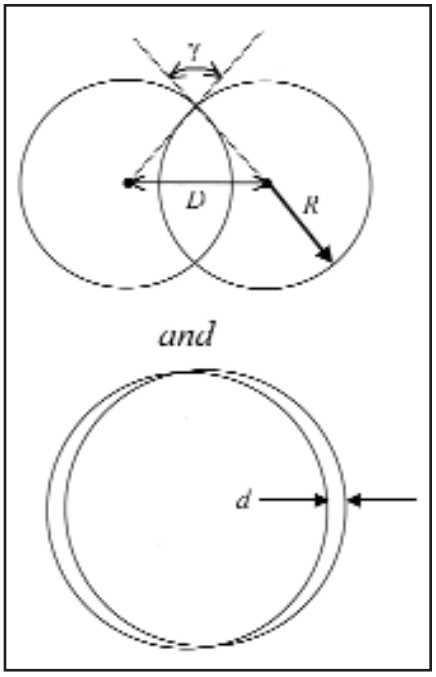

Fig. 3 — Important geometrical parameters that determine the intersection problem.

Another shortcoming addressed in this work is the fact that current pore closure models portray weld surface topography too simplistically: actual engineering surfaces are not ideal arrays of pores. Although recognized by some workers (e.g., Ref. 14), to date there has not been a method proposed to account for this topographic variability. This work addresses surface topography in two ways. Firstly, the statistical problem of randomly intersecting circular machining marks is solved. Secondly the surface roughness on a microscopic scale is specified by distribution functions, and the nonlinear ordinary differential equations (ODE) in pore closure models then operate on such distributions. This is accomplished by a Monte Carlo method (see Appendix). It should be noted the proposed framework can be used to model any manufacturing uncertainty/variability including material properties, boundary conditions, etc. The physical phenomena not addressed in this work include weld contamination, material texture, residual stresses, and the effect of microstructural evolution on creep.

Probabilistic Approach to Pore Closure Models — Problem Formulation

The problem of weld surface topography will now be addressed. The idealized but incorrect representation of the weld plane is shown in Fig. 2A. Real surfaces are typically prepared using circular motion and a cutting tool with some specified cutting speed (surface velocity of tool relative to workpiece) and feed rate (distance between adjacent engagements of tool and workpiece). The part is generally larger than the cutting tool path and therefore the intersection of cutting tool marks from adjacent cuts is better represented by Fig. 2B. The black lines are cutter marks on one faying surface intersecting at some angle the gray machining marks on the opposite surface. It is assumed in this work that these circular marks randomly intersect. In addition to the intersection of cutter lines, other manufacturing attributes determining initial porosity distribution include the feed and the surface roughness. To a first approximation these three local surface quantities, feed, roughness,

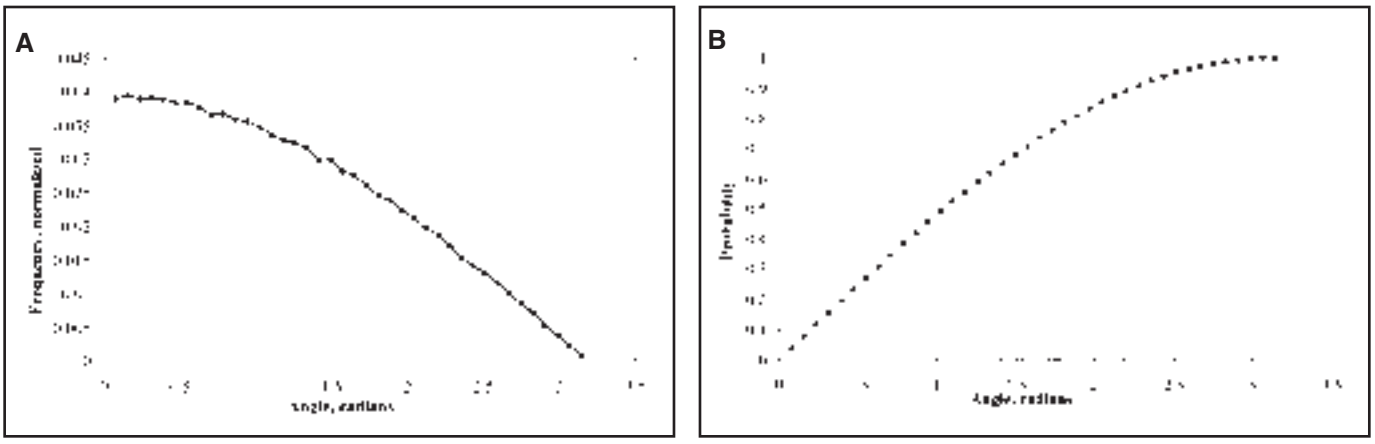

Fig. 4 — Intersection of cutter marks. A — Normalized PDF for angle of intersection γ; B — CDF corresponding to PDF shown in Fig. 4A.

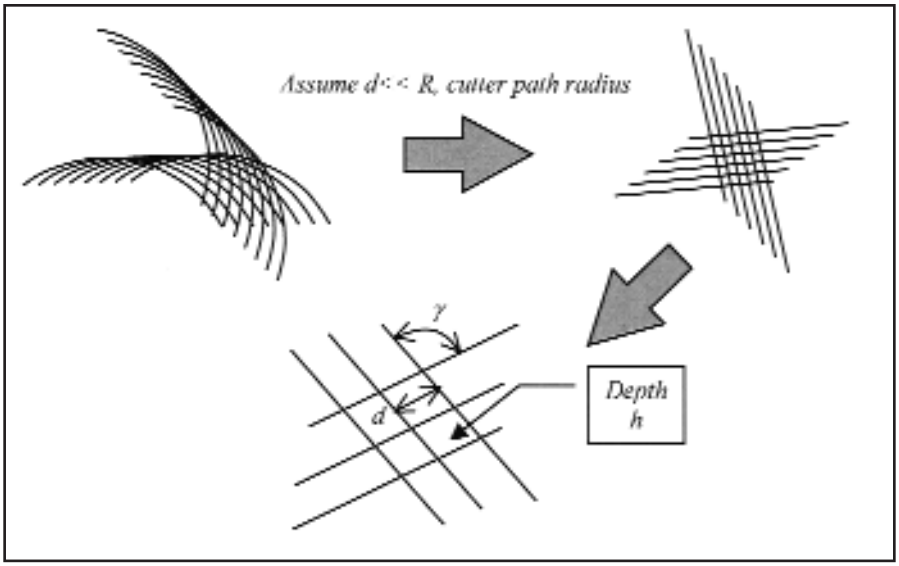

Fig. 5 — Initial porosity distribution locally described as arrays of ellipsoidal pores.

and the intersection angle, determine the distribution of initial voids.

The prototypical intersection event occurs when two circular marks cross, as shown in Fig. 3. The important variables are the center-to-center spacing D, the cutter radius R, intersection angle γ, and the feed spacing d when considering the marks immediately adjacent to the two intersecting circles. From elementary geometry, we see that

$$\gamma = 2 \cdot \tan^{-1}\left\{\left[\left(\frac{1}{\phi}\right)^2 - 1\right]^{-\frac{1}{2}}\right\}$$

where R is the cutter path radius, and

$$\phi \equiv \frac{D}{2R}, 0 < \phi < 1 \quad (1)$$

Since the circles are assumed to intersect

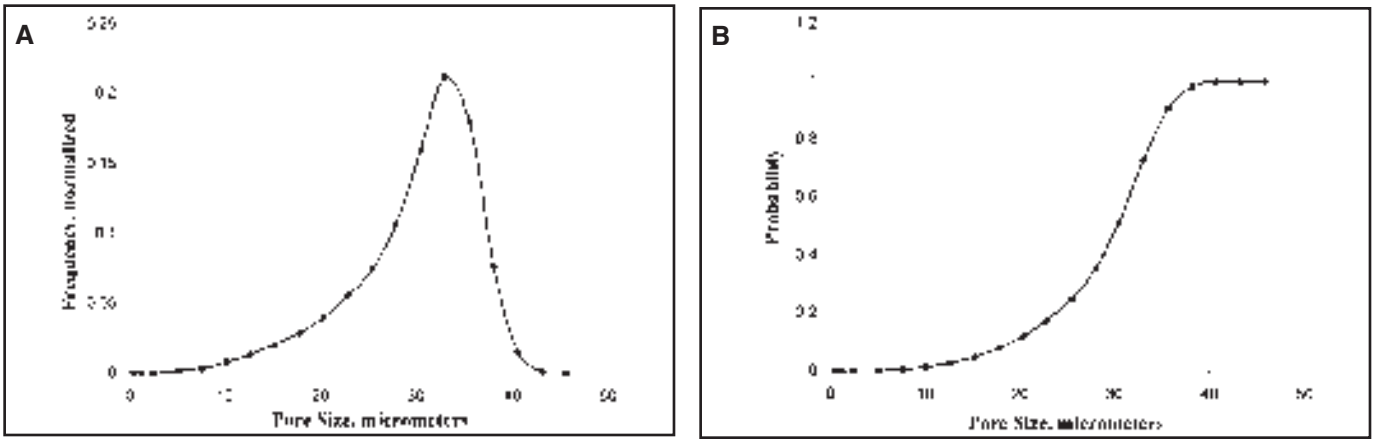

Fig. 6 — Initial pore distribution. A — Example of a normalized PDF for initial pore size; B — CDF corresponding to PDF shown in Fig. 6A.

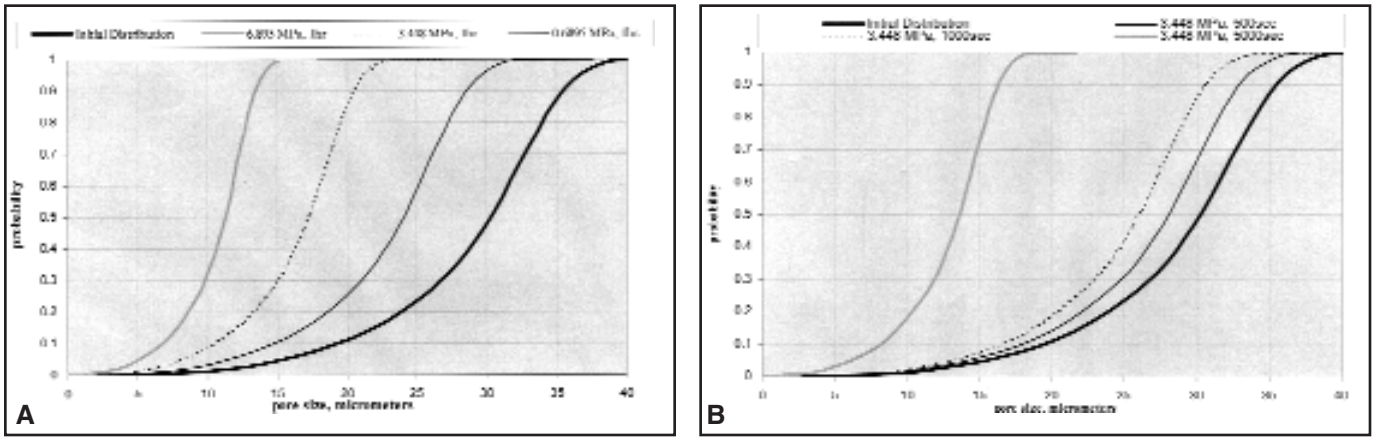

Fig. 7 — Evolution of pore size distribution. A — As a function of externally applied weld pressure; B — as a function of weld time at a given applied pressure.

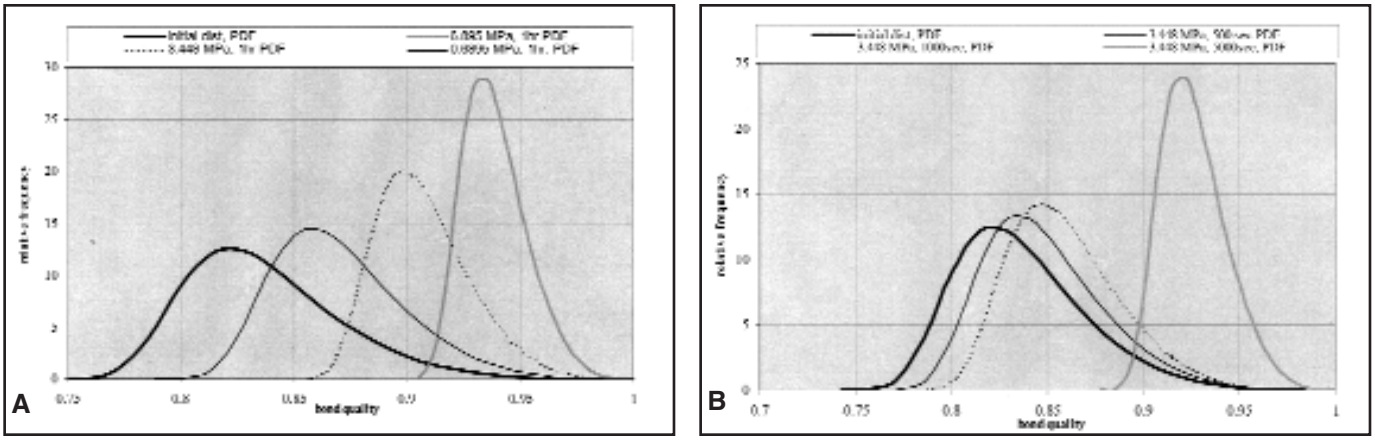

Fig. 8 — PDFs showing evolution of weld quality. A — As a function of applied pressure; B — as a function of weld time at a given pressure.

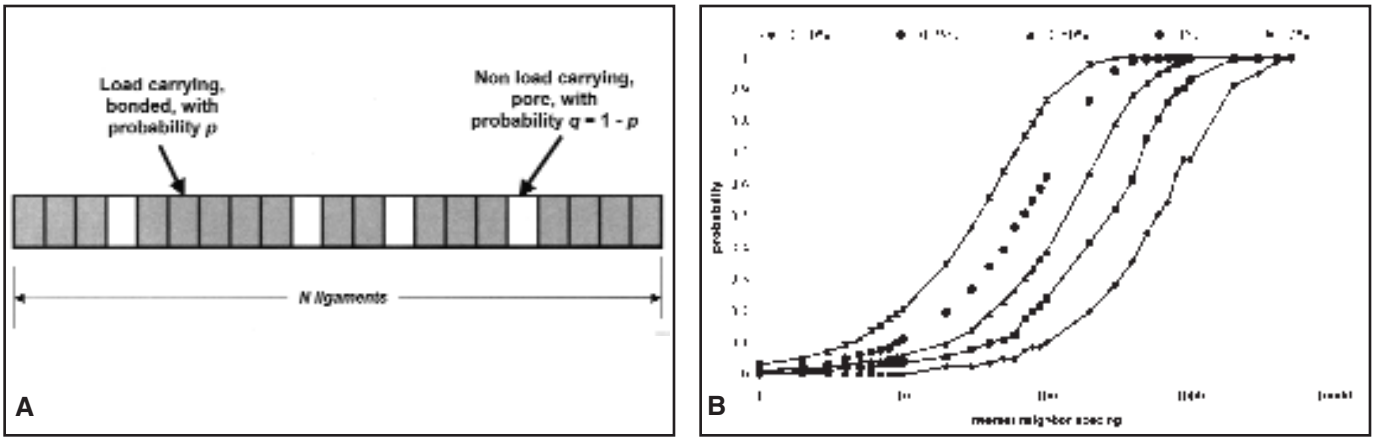

Fig. 9 — Schematic of 1-D lattice model of a diffusion weld. A — Welded vs. unwelded elements; B — CDFs for pore nearest neighbor spacing as a function of porosity level.

Table 2 — Material Constants Used in Modeling Pore Closure

Material Constant	Numerical Value (cgs units)
γ, pore surface energy	1000 erg/cm^2
D, diffusivity	10^{-9} cm^2/s
K_1, material parameter in constitutive equation for material creep	4.235×10^{-12} (dynes/cm^2)$^{-1}$ * (s)$^{-1}$
σ_0, material parameter in constitutive equation for material creep	3.275×10^{-6} (dynes/cm^2)
Ω, vacancy volume	2.7×10^{-23} cm^3
B, vacancy sink radius (assumed to be identical to average value of the feed spacing d)	0.01778 cm

at random on the weld plane, ϕ may be thought of as a uniform random variable on the interval [0,1]. Equation 1 then generates the probability density function (*PDF*) and the cumulative distribution function (*CDF*) for the angle of intersection γ. The *PDF* is the frequency of occurrence of a particular quantity, whereas the *CDF* is the probability that the given quantity will assume a value less than or equal to a specified value. A Monte Carlo method as described in the Appendix is used to perform the evaluation. The histogram bin size for the angle γ is 0.025π over the range $[0,\pi]$. The resulting normalized *PDF* and *CDF* for the angle of intersection γ are shown in Fig. 4A and 4B, respectively. These calculated distribution functions are continuous but "serrated" on account of the finite bin size. These distributions are independent of cutter size and are valid as long as the assumption of random intersection is met.

The feed d is assumed to obey a distribution function as well. Typical feed rates for the finish machining of titanium are on the order of 178 micrometers/rev (0.007 in./rev) (Ref. 27). The feed rate varies due to vibration in the tool or fixture, tool wear, and material hardening during cutting and residual stress-induced surface deformation. In practice the distribution function for the feed spacing can be experimentally determined from surface profile traces measuring the distribution of peak-to-peak spacing. Similarly, the initial void depth h is correlated to the surface roughness of the as-machined surface as well as subsequent steps such as chemical cleaning. In this work it will be assumed that both d and h are normally distributed.

Using the relationship in Equation 1 and assuming d and h follow normal distribution laws, the initial distribution of porosity is calculated, i.e., initial conditions for pore closure models. Figure 5 illustrates that if the feed is much smaller than the cutter path radius R, then the local surface intersection problem is reduced to the problem of an array of ellipsoidal pores specified by d, h, and γ. In this work a further simplifying assumption will be made: "equivalent" spherical pores are assumed because the model by Garmong

et al. (Ref. 8) used in subsequent calculations is only valid for spherical pores. The models of Derby and Wallach (Refs. 11–14) and Hill and Wallach (Ref. 15) are capable of handling elliptical pores. More complex models would be a numerical extension of this work without significant qualitative differences. The equivalent spherical pore radius will be taken as the radius of a spherical pore with the same volume as an ellipsoid.

$$r_{equiv} = \sqrt[3]{hd^2 \cos\left(\frac{\gamma}{2}\right) \cdot \sin\left(\frac{\gamma}{2}\right)} \qquad (2)$$

Figure 6A shows the normalized *PDF* for the initial pore size assuming the following: d_{mean} = 178 micrometers (0.007 in.) with an assumed standard deviation of 17.8 micrometers (0.0007 in.), h_{mean} corresponds roughly to R_{max} *and* R_{max}, ≈ 2.54 micrometer (100 microinch), and the standard deviation for h is assumed to be 0.254 micrometer (10 microinch). Figure 6B shows the corresponding *CDF*. Note the skew-type asymmetry of this distribution.

Next, the initial pore size distribution is incorporated into mechanistic models for pore closure. The initial pore size is assumed to be a continuous random variable with distributions as described by Fig. 6A and 6B. The final pore size will therefore be a function of this random variable, also depending on parameters such as pressure and temperature. To find the distribution function for the final pore size given the distribution for the initial pore size, the following identity is invoked (Ref. 28):

$$\begin{aligned} &\textit{Given random variable } X \textit{ and} \\ &\textit{a function } Y \equiv g(X) \\ &\textit{where } g(X) \textit{ is a monotonic} \\ &\textit{function of } X, \textit{ then} \\ &CDF_Y(t) \equiv P(Y \le t) \\ &\quad = P\left(X \le g^{-1}(t)\right) \\ &\quad \equiv CDF_x\left(g^{-1}(t)\right) \end{aligned} \qquad (3)$$

For the simple case in which the final pore size depends only on the initial pore size with pressure, temperature, etc., appearing as fixed parameters, equating probabilities for equivalent events as formally described in Equation 3 is valid. In this case the function g is the solution to the ODEs for pore closure. If, however, pressure and temperature also obey distributions, or if more complex models are used involving more than one random variable, Equation 5 cannot be used because there will be multiple ways to create equivalent outcomes. In such cases, a Monte Carlo approach is used — Fig. A1.

As previously mentioned, the model used in this work is due to Garmong et al. (Ref. 8). This model is described by the ODEs below

$$\left(\frac{da}{dt}\right)_{TOTAL} = \left(\frac{da}{dt}\right)_{CREEP} + \left(\frac{da}{dt}\right)_{DIFFUSION} \qquad (4)$$

where a is the pore size and t is the elapsed time.

The creep and diffusion contributions are specified by

$$\left(\frac{da}{dt}\right)_{DIFFUSION} = -\left(\frac{D\Omega}{kT}\right) \cdot \frac{d}{a(d-a)} \cdot \left[\frac{2\gamma}{a} + P_{ext}\right] \qquad (5a)$$

where D is the diffusion constant (self-diffusion for vacancies); Ω is the vacancy volume; k is Boltzmann's constant; T is the absolute temperature; d is the spacing between pores, i.e., the feed rate; γ is the pore surface energy; and P_{ext} is the externally applied stress.

$$\left(\frac{da}{dt}\right)_{CREEP} = -\frac{3K_1 a}{4} \left\{2\sigma_o \ln\left(\frac{d}{a}\right) + \left(\frac{2\gamma}{a} + P_{ext} - P_{int}\right)\right\} \cdot \left(1 - \frac{a^3}{d^3}\right)^{-1} \qquad (5b)$$

where K_1 is a material constant in a constitutive creep model described in Ref. 8; σ_o is also a material constant in a constitutive creep model described in Ref. 8; d is the spacing between pores, i.e. the feed rate; and P_{int} is the pressure inside the pore due to trapped residual gas.

These equations were solved using a fourth-order Runge-Kutta method (Ref. 29) with fixed step size. The material constants used from Ref. 8 are reproduced in Table 2. Equations 5a and 5b were numerically integrated using the initial pore size distribution shown in Fig. 6A. For a given initial pore size, the final pore size was calculated. The probability associated with the given initial pore size as in Fig. 6B was also assigned to the corresponding final pore size to create the *CDF* for final pore size in accordance with Equation 3.

Probabilistic Approach to Pore Closure Models — Model Results

The resulting *CDF*s for final pore size are shown in Fig. 7A for various levels of applied external load, namely 0.6895 MPa (100 lb/in.^{2}), 3.448 MPa (500 lb/in.^{2}), and 6.895 MPa (1000 lb/in.^{2}) at a weld time of one hour. Alternatively at a stress of 3.448 MPa, the effect of varying weld time is shown in Fig. 7B. These *CDF*s were then fitted to the following functional form using a nonlinear least squares algorithm:

$$G(z) = erf\left[A \cdot z^B\right] \qquad (6)$$

where A and B are parameters and *erf* is the error function.

The resulting fitted *CDF*s were differentiated to get the corresponding *PDF*s, as shown in Fig. 8A and B. Figures 8A and B show *PDF*s with equivalent weld quality shown on the abscissa. This quality was calculated as follows:

$$\begin{aligned} &\textit{for any given pore size,} \\ &\textit{porosity fraction} = \frac{a}{d} \\ &\textit{equivalent weld quality} = 1 \\ &- \textit{porosity fraction} = 1 - \frac{a}{d} \end{aligned} \qquad (7)$$

As weld quality improves, the *PDF*s become more sharply peaked — a phenomenon observed in actual production situations (Ref. 30). It is, therefore, seen that even a simple mechanistic pore closure model, when combined with the probabilistic framework proposed herein, produces results representative of production situations. The link to impact strength is equally important and will now be established.

Statistical Models for Composite Strength and Their Applicability to Modeling Impact Strength for Diffusion Welded Components

The strength model used is due to Phoenix and Beyerlein (Refs. 31, 32), who developed a series of probabilistic models for the failure of composites by considering load-sharing effects, random strength flaws, and clustering of failure sites. One model in particular (Ref. 31) predicts the *CDF* for strength of a 1-D "weld line" consisting of an initial distribution of intact welded ligaments and broken ligaments or pores. This model may also be used to model impact tests performed on diffusion welded Ti-6Al-4V because (Ref. 33) of the following:

■ High strain rate or high rate of load-

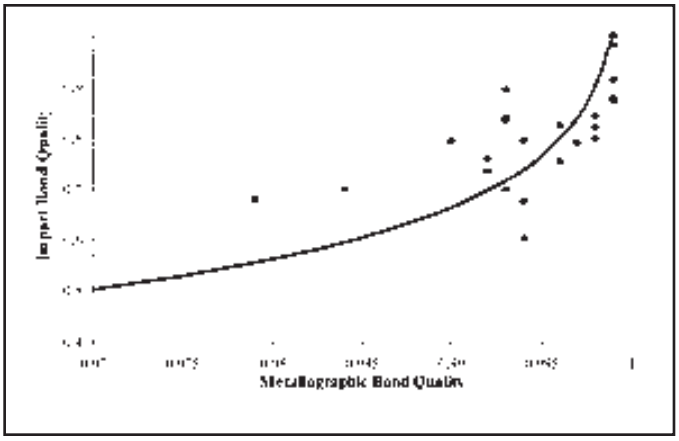

Fig. 10 — Comparison between Equation 9 (solid line) and data for diffusion welds in Ti-6Al-4V.

ing is conducive to brittle fracture.

■ Brittle fracture can more readily occur in materials with low notch toughness such as high-strength Ti-alloys.

■ The presence of flaws such as residual weld-interface porosity exacerbates the tendency towards brittle fracture and leads to variations in strength from one weld to another.

It is, therefore, a reasonable approximation to apply a probabilistic failure model developed for composites to the case of interest here.

The strength model used in this work is based on the clustering of defects (pores) and the effect of such clusters on component strength. The model, therefore, emphasizes the local interaction among defects as eventually resulting in global failure. To understand just how quickly pore clustering develops, consider a simple numerical experiment on a 1-D lattice. Suppose each point is a welded ligament or a pore as schematically shown in Fig. 9A. Now consider what happens when porosity is introduced at random sites with a probability of occurrence ranging from 0.001 to 0.02. The resulting *CDF*s showing the nearest neighbor spacing are shown in Fig. 9B. It is seen the pore spacing decays very rapidly as the porosity level increases and the number of clustered pores goes up significantly.

The detailed derivation for the strength model is beyond the scope of this article but is found in Refs. 31 and 32. The essential concepts are as follows:

■ The diffusion weld is a lattice of intact and broken ligaments; the broken ligaments are pores.

■ A 1-D row of weld ligaments is considered with probability p that a weld ligament will be intact (full strength) and probability $1–p = q$ that it will be a pore (nil strength).

■ Tapered load sharing is assumed: a pore distributes ⅔ of the load it would have carried to the nearest neighbor and ⅓ to the next-nearest neighbor.

■ Local failure configurations are considered in detail for a 1-D lattice, and their probabilities of occurrence are determined.

■ The distribution function for strength is estimated with special attention to the asymptotic behavior for large numbers of ligaments.

The principal result used in this work is given by Equation 78b from Ref. 31, which gives the strength of a 1-D lattice in the asymptotic limit for large lattice sizes.

$$\textit{failure load} \propto \frac{-ln\left(q^2\delta\right)}{ln\left(n\right)}, \qquad \delta \approx \sqrt{q} + q/2 \tag{8}$$

where n is the lattice size of weld ligaments, q is the probability of occurrence of a pore, and δ is the solution of a characteristic equation describing certain key local failure configurations (clustering of defects).

At some residual porosity level the weld impact properties approach that of base metal. For the Ti-6Al-4V diffusion welds herein, this is experimentally found to be approximately 0.1%, or $q = 0.001$. The quantity of interest is therefore the failure load in comparison to that of base material, namely the ratio

$$Q \equiv ln\left(q^2\delta\right) \Big/ \left[ln\left(q^2\delta\right)\right]_{q=0.001} \tag{9}$$

This ratio Q is the weld quality as determined by impact testing and is related through Equations 10 and 11 to the metallographic weld quality, namely $1-q$. Also note this equation is independent of the size of the welded area. The result of plotting Equation 9 against actual data from diffusion welds made in Ti-6Al-4V is shown in Fig. 10. The material used was AMS 4928 with welding conditions as follows: weld pressures of 1.379–13.79 MPa (200–2000 lb/in.^{2}), time of 1–3 hours, and temperatures of 871°C–982°C (1600°F–1800°F). It is seen that Equation 9 models the relationship between metallographic quality and impact quality reasonably well. The most significant limitation of the current strength model is it is 1-D.

Conclusions

This work has extended current modeling approaches for diffusion welding by implementing the following:

1) A probabilistic framework tracking the evolution of porosity distributions and incorporating the effects of weld process parameters and manufacturing process attributes

2) This modeling framework allows mechanistically-based pore closure models to be effectively applied to real manufacturing situations

3) The probabilistic pore closure modeling approach realistically describes the evolution of metallographic weld quality as observed in manufacturing practice, namely that as the weld quality improves the *PDF*, representing metallographic weld quality, becomes more narrowly distributed about its mean

4) A probabilistic failure model is used to successfully model the relationship between metallographic weld quality and impact weld quality as measured by fraction of base metal impact strength

The modeling framework presented here therefore accomplishes the said objective of linking weld impact strength and weld process attributes through a probabilistic treatment of the evolution of porosity distributions. The approach is general and may be used with any pore closure model. Future work required to further validate this modeling approach includes additional experimental verification and utilization of other pore closure models such as those by Derby and Wallach (Refs. 11–14) and Hill and Wallach (Ref. 15). Additionally, a method of extracting 2-D and 3-D surface topography parameters directly from measurements is desirable, going beyond simple notions of R_a and capturing higher dimensional features of real surfaces. Other uses for the model include performing various tradeoff studies. For example, for a certain required level of weld quality, a constrained optimization problem examines tradeoffs between pressure, temperature, time, and surface finish.

Acknowledgments

The Los Alamos authors would like to acknowledge the support of the U.S. Dept. of Energy (DoE) and the University of California, which operates Los Alamos National Laboratory for DoE under contract W-7405-ENG-36. The authors also

wish to thank R. D. Dixon for his critical review of the manuscript.

References

1. Cogan, R. M., and Shamblem, C. E. 1969. Development of a manufacturing process for fabricated diffusion bonded hollow blades. Technical Report AFML-TR-69-219.

2. Fitzpatrick, G. A., and Broughton, T. 1988. Diffusion welding aeroengine components. *Defense Science Journal* 38(4): 477–486.

3. Weisert, E. D. 1988. Hollow titanium turbofan blades. *Superplasticity in Aerospace*, eds. H. C. Heikkenen and T. R. McNelley, pp. 315–329. The Metallurgical Society (TMS) Press.

4. Barth, C. F. 1992. Rotating components — a challenge for SPF/DB. Society for Manufacturing Engineers, SME Technical Paper MF92-188.

5. King, W. H., and Owczarski, W. A. 1968. Additional studies on the diffusion welding of titanium. *Welding Journal* 47(10): 444-s to 450-s.

6. Kellerer, H., and Milacek, L. H. 1970. *Welding Journal* 49(5): 219-s.

7. Hamilton, C. H. 1973. Pressure requirements for diffusion bonding titanium. *2nd Intl. Conf. on Titanium Science and Technology*, eds. R. I. Jaffee and H. M. Burte, pp. 625–648. Plenum Press.

8. Garmong, G., Paton, N. E., and Argon, A. S. 1975. Attainment of full interfacial contact during diffusion bonding. *Metallurgical Transactions A*, 6A(6): 1269–1279.

9. Coble, R. L. 1970. Diffusion models for hot pressing with surface energy and pressure effects as driving forces. *J. of Applied Physics* 41(12): 4798–4807.

10. Wilkinson, D. S., and Ashby, M. F. 1975. Pressure sintering by power law creep. *Acta Metallurgica* 23(11): 1277–1285.

11. Derby, B., and Wallach, E. R. 1982. Theoretical model for diffusion bonding. *Metal Science* 16(1): 49–56.

12. Derby, B., and Wallach, E.R. 1984. Diffusion bonding: development of theoretical model. *Metal Science* 18(9): 427–431.

13. Derby, B., and Wallach, E. R. 1984. Diffusion bonds in copper. *J. of Materials Science* 19: 3140–3148.

14. Derby, B., and Wallach, E. R. 1984. Diffusion bonds in iron and a low-alloy steel. *J. of Materials Science* 19: 3149–3158.

15. Hill, A., and Wallach, E. R. 1989. Modeling solid-state diffusion bonding. *Acta Metallurgica* 37(9): 2425–2437.

16. Pilling, J., Livesey, D. W., Hawkward, J. B., and Ridley, N. 1984. Solid state bonding in superplastic Ti-6Al-4V. *Metal Science* 18(3): 117–122.

17. Guo, Z. X., and Ridley, N. 1987. Modeling of diffusion bonding of metals. *Materials Science and Technology* 3(11): 945–953.

18. Takahashi, Y., and Inoue, K. 1992. Recent void shrinkage models and their applicability to diffusion bonding. *Materials Science and Technology* 8(11): 953–964.

19. Grigor'evskii, V. I., and Karakozov, E. S. 1983. Method of reducing the residual strains in components of titanium alloys in diffusion bonding. *Welding Production (Svarochnoe Proizvodstvo)* 30(2): 19– 21.

20. Peshkov, V. V., Rodionov, V .N., and Nikgolov, M. B. 1985. Diffusion bonding of titanium with low stored strain in bonded components. *Welding Production (Svarochnoe Proizvodstvo)* 32(9): 19–21.

21. Nikgolov, M. B., Peshkov, V. V., and Rodionov, V. N. 1986. Relationships governing formation of the microrelief on the surface of titanium alloys in diffusion bonding conditions. *Welding Production (Svarochnoe Proizvodstvo)* 33(3): 45–47.

22. Karakozov, E. S., Ternovskii, A. P., and Lavrov, B. A. 1983. Effect of the rolling texture on the formation of the bond in diffusion bonding titanium alloys. *Welding Production (Svarochnoe Proizvodstvo)* 30(7): 39–41.

23. Peshkov, V. V., Milyutin, V. N., and Podoprikhin, M. N. 1984. Interaction of titanium with residual gases in the evacuated space in conditions of diffusion bonding. *Welding Production (Svarochnoe Proizvodstvo)* 31(2): 21–23.

24. Peshkov, V. V., Kholodov, V. P., and Vorontsov, E. S. 1985. Kinetics of dissolution of oxide films in titanium in diffusion bonding. *Welding Production (Svarochnoe Proizvodstvo)* 32(4): 49–51.

25. Peshkov, V. V., Podoprikhin, M. N., and Milyutin, V. N. 1984. Effect of oxide films on the interaction between contact surfaces in diffusion bonding of titanium. *Welding Production (Svarochnoe Proizvodstvo)* 30(12): 8–9.

26. Ohsumi, M., Kiyotou, S.-I. and, Sakamoto, M. 1985. The application of diffusion welding to aircraft titanium alloys. *Trans. of the Iron and Steel Institute of Japan* 25(6): 513–520.

27. Schey, .J.A. 1987. *Introduction to Manufacturing Processes*, 2nd ed. New York, N.Y.: McGraw-Hill Book Co.,

28. Larson, H. J. 1982. *Introduction to Probability Theory and Statistical Inference*, 3rd ed. New York, N.Y.: John Wiley & Sons.

29. Hildebrand, F. B. 1974. *Introduction to Numerical Analysis,* 2nd ed. New York, N.Y.: Dover Publications, Inc.,

30. Private Communication, 1999. United Technologies Corporation, East Hartford, Conn.

31. Phoenix, S. L., and Beyerlein, I. J. 2000. Distribution and size scalings for strength in a one-dimensional lattice with load redistribution to nearest and next-nearest neighbors. *Physical Review E* 62(2): 1622–1645.

32. Phoenix, S. L., and Beyerlein, I. J. 2001. Statistical strength theory for fibrous composite materials. *Comprehensive Composites 1*. Edited by T. W. Chou and C. Zweben. Pergamon Press, pp. 559–639.

33. Dieter, G. E. 1986. *Mechanical Metallurgy*, 3rd ed., New York, N.Y.: McGraw Hill Book Co.,

34. Metropolis, N., and Ulam, S. 1949. The Monte Carlo method. *J. of the American Statistical Asso*ciation, 44(247): 335–341.

35. Shreider, Y. A., ed. 1966. *The Monte Carlo Method — The Method of Statistical Trials. 1996. Edited by Y. A. Schreider* Oxford, U.K.: Pergamon Press.

Appendix

A Concise Overview of the Monte Carlo Method

The Monte Carlo method of statistical trials was invented at Los Alamos National Laboratory (Refs. 34, 35) to solve complex physical problems in an era before powerful computers. The method assumes the existence of a set of random numbers and a set of probabilities describing the occurrence of given events. Suppose there are j such discrete events, each with probability of occurrence p_j. If we assume at least one of these events must occur, then

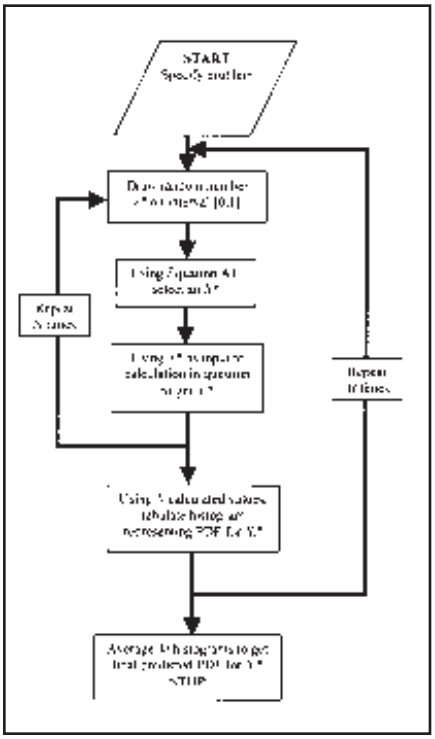

Fig. A1 — Flowchart of Monte Carlo computational approach.

$$\sum_{j=1}^{J} p_j = 1 \qquad \text{(A1)}$$

If the probabilities are arranged on the interval [0,1], and if we choose a random number r on the same interval, then the

Monte Carlo method assumes event j is "selected" if

$$\sum_{n=1}^{j-1} p_n \le r \le \sum_{n=1}^{j} p_n \qquad \text{(A2)}$$

This is also known as a "roulette wheel" method of selection.

In this work, we take the limit as the bin size or the width of the slots on the roulette wheel get very small and the distribution of probabilities on the interval [0,1] becomes continuous. Then, for a given random variable X, we assume the value X^* is selected for the calculation if for a given random number r^*

$$X^* \text{ is chosen if } r^* = CDF_X(X^*) \qquad \text{(A3)}$$

The flowchart in Fig. A1 schematically shows what happens after the selection process. The value of X^* is taken as an input to the problem, e.g., the *ODE* describing pore closure. In that case, the final pore diameter X_f^* is the output. The selection process is then repeated and a new final pore size is calculated and so on.

This is repeated for N trials, and M runs of N trials are done to get adequate averaging statistics. The *PDF* for the final pore size X_f^* is assembled by tabulating the M histograms from each run and averaging them. This can be repeated for various initial pore size distributions and values of the process variables to completely characterize the way in which the final pore size distribution evolves as a function of manufacturing process attributes. Although the case shown here is for only one random variable, the more general case of multiple random variables can also be handled by the Monte Carlo method. For example, pressure, temperature, and even material properties could all be represented by distribution functions in the same manner as initial pore size.

Preparation of Manuscripts for Submission to the *Welding Journal* Research Supplement

All authors should address themselves to the following questions when writing papers for submission to the Welding Research Supplement:

- Why was the work done?
- What was done?
- What was found?
- What is the significance of your results?
- What are your most important conclusions?

With those questions in mind, most authors can logically organize their material along the following lines, using suitable headings and subheadings to divide the paper.

1) **Abstract.** A concise summary of the major elements of the presentation, not exceeding 200 words, to help the reader decide if the information is for him or her.

2) **Introduction.** A short statement giving relevant background, purpose, and scope to help orient the reader. Do not duplicate the abstract.

3) **Experimental Procedure, Materials, Equipment.**

4) **Results, Discussion.** The facts or data obtained and their evaluation.

5) **Conclusion.** An evaluation and interpretation of your results. Most often, this is what the readers remember.

6) **Acknowledgment, References and Appendix.**

Keep in mind that proper use of terms, abbreviations, and symbols are important considerations in processing a manuscript for publication. For welding terminology, the *Welding Journal* adheres to AWS A3.0:2001, *Standard Welding Terms and Definitions.*

Papers submitted for consideration in the Welding Research Supplement are required to undergo Peer Review before acceptance for publication. Submit an original and one copy (double-spaced, with 1-in. margins on 8 ½ x 11-in. or A4 paper) of the manuscript. Submit the abstract only on a computer disk. The preferred format is from any Macintosh® word processor on a 3.5-in. double- or high-density disk. Other acceptable formats include ASCII text, Windows™, or DOS. A manuscript submission form should accompany the manuscript.

Tables and figures should be separate from the manuscript copy and only high-quality figures will be published. Figures should be original line art or glossy photos. Special instructions are required if figures are submitted by electronic means. To receive complete instructions and the manuscript submission form, please contact the Peer Review Coordinator, Doreen Kubish, at (305) 443-9353, ext. 275; FAX (305) 443-7404; or write to the American Welding Society, 550 NW LeJeune Rd., Miami, FL 33126.